Journal of Alloys and Compounds 509 (2011) 7100–7104

Contents lists available at ScienceDirect

Journal of Alloys and Compounds

journal homepage: www.elsevier.com/locate/jallcom

Optical properties of Si–N doped $BaMgAl_{10}O_{17}:Eu^{2+}$, Mn^{2+} phosphors for plasma display panels

Bitao Liu, Feng Zhang, Ge Zhu, Yan Wen, Shuangyu Xin, Wenjie Wang, Yuhua Wang*

Department of Materials Science, School of Physical Science and Technology, Lanzhou University, Lanzhou 730000, PR China

ARTICLE INFO

Article history:
Received 30 January 2011
Received in revised form 29 March 2011
Accepted 2 April 2011
Available online 9 April 2011

Keywords:
PDP
$BaMgAl_{10}O_{17}$
Thermal stability

ABSTRACT

The photoluminescence properties of Si–N doped $BaMgAl_{10}O_{17}:Eu^{2+}$, Mn^{2+} phosphors were studied. Photoluminescence spectrum, powder X-ray diffraction and decay curves were used. The electronic structure of un-doped $BaMgAl_{10}O_{17}$ was investigated by using the density functional theory. It reveals that an ideal hexagonal shape and particle size in 3–5 μm are obtained by Si–N doping. Additionally, its photoluminescence and thermal stability are both improved. The energy transfer from Eu^{2+} to Mn^{2+} also enhanced by suitable Si–N doping. These are expected to be potentially applicable to industrial production of the phosphor in plasma display panels.

1. Introduction

Europium-doped barium magnesium aluminates phosphor (BAM) has been widely used as a blue component in various luminescent applications such as three-band fluorescence lamps, plasma display panels and Hg-free lamps due to its high luminance efficiency and good color purity under ultraviolet (UV) and vacuum ultraviolet (VUV) excitation [1–4]. However, its luminescence intensity is distinctly decreased by heat treatment during the manufacturing process. This deterioration is one of the most significant shortcomings in the application [5–9].

Up to now, the luminance decrease of BAM encountered in manufacturing is generally considered to be thermal degradation, because it accompanies thermal annealing in oxidizing atmosphere. It is generally agreed that thermal degradation of BAM occurs by oxidation of divalent Eu to its trivalent form due to the adsorbed oxygen atom diffused into the conduction layer accompanied by the oxygen vacancies, several possible interpretations regarding the detailed oxidation mechanism have been reported [5,6,8]. On the other hand, some studies suggested that the thermal degradation was due to a structural change such as an altered local environment for the Eu^{2+} ions and the migration of Eu^{2+} ions [7,9,10]. In our previous work, it has been confirmed that restricting the migration of Eu^{2+} from mirror planes to spinel blocks is an efficient way to improve the thermal stability [11].

As shown, in Fig. 1, BAM crystallizes in the β-Al_2O_3 structure with the space group $P_{63}mmc$, which is similar to ion conductor of $NaAl_{11}O_{17}$. Al^{3+} ions and O^{2-} ions formed a 3D network structure as AlO_4 tetrahedron and AlO_6 octahedron in spinel block, and Mg^{2+} ions occupied one Al site in a unit cell. Ba^{2+} ions and O^{2-} ions occupy the conduction layer sites which connected two spinel layers as exhibited in Fig. 1. Clearly, the conduction layer did not formed as a compact 3D network structure as the spinel blocks exhibited. For this reason, it would lead the instability of the O (1) sites localized in the conduction layer. It is very likely that oxygen ions localized at O (1) sites marked in Fig. 1 would miss for the phosphor have to synthesize in a reduction atmosphere, and an oxygen vacancy could be generated [12–14]. On the other hand, these oxygen ions (localized at O (1) sites) may get into the interstitial site in conduction layer which is called Reitinger defect with a corresponding migration of Al^{3+} to form Al_i–O_i–Al_i bridges between the spinel blocks would be generated [10,14]. These two types of defects would accelerate the luminescence degradation. Thus, it is a critical issue to improve the stability of the AlO_4 tetrahedra which marked with solid tetrahedra (with no atom bond in the tetrahedra) in Fig. 1. It is reported that co-doping Si^{4+} can efficiently reduce the lattice parameter and enhance the emission intensity [4]. But unfortunately, due to the unequal charge replacement, it also induces a worse thermal stability. To maintain the electrical neutrality of the compounds, an ion with three negative charges should be combined with Si^{4+}, which should occupy the nearby oxygen ions. To our best knowledge, it is intriguing to note that Si–N in Si_3N_4 always formed as a Si–N tetrahedral and it can withstand a high temperature more than 1400 °C [15,16]. Another information we should emphasize that the bond lengths for tetrahedral Si–N bonds (168.5–176 pm in Si_3N_4) is

* Corresponding author. Tel.: +86 931 8912772; fax: +86 931 8913554.
E-mail address: wyh@lzu.edu.cn (Y. Wang).

0925-8388/$ – see front matter © 2011 Elsevier B.V. All rights reserved.
doi:10.1016/j.jallcom.2011.04.011

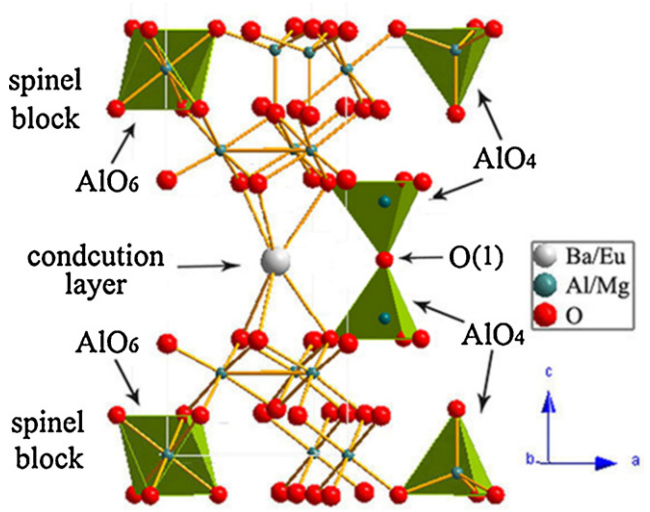

Fig. 1. Crystal structure of $BaMgAl_{10}O_{17}$. Only half of the unit cell (c = 0 to 1/2) is shown.

almost equal to versus tetrahedral Al–O bonds (176.1 pm in BAM) [15,16], which means that suitable Si–N doping would not change the lattices.

On the other hand, the extreme difference in degradation between different host phosphors will produce color aberration, and it is important to investigate a single-host phosphor with various emission bands. BAM:Mn is considered as a green phosphor for PDPs due to its high VUV efficiency and excellent green color point, though most PDP manufacturers presently still apply Zn_2SiO_4: Mn due to its better VUV stability [17]. Therefore, this work focuses on the development of luminescence properties of single host BAM:Eu^{2+}, Mn^{2+} co-doped with Si_3N_4. Its luminescence properties, morphology and particularly energy transfer were investigated. In addition, the electronic structure of BAM was calculated by density functional theory calculation. These properties are particularly important for the phosphor for plasma panel displays.

2. Experimental

2.1. Materials and synthesis

The BAM phosphor with 10 mol% Eu^{2+} and 12 mol% Mn^{2+} was synthesized by solid-state reaction according to our previous work. A stoichiometric mixture of $BaCO_3$ (99.99%), MgO (99.99%), Al_2O_3 (99.99%), Si_3N_4 (99.9%), $C_6H_9MnO_6{\cdot}2H_2O$ (99.99%) and Eu_2O_3 (99.99%) was ground with 3 wt% Li_2CO_3 (99%) and 3 wt% BaF_2 (99%) as a flux. Then the milled starting materials were fired at 1450 °C in a reducing atmosphere (5% H_2 and 95% N_2 mixture gas) for 4 h. For investigating the thermal stability, samples were annealed in air atmosphere for 1 h.

2.2. Characterization

Phase identification of samples was carried out by a Rigaku D/Max-2400 X-ray diffractometer with Cu Kα radiation. The morphology of the powders was examined with a JEOL-5600 scanning electron microscope (SEM). The PL spectra in the UV region were obtained by a FLS-920T fluorescence spectrophotometer equipped with Xe 900 (450 W xenon arc lamp) as the light source with spectral slits width of 0.5 nm. All the measurements were performed at room temperature.

2.3. Computational detail

The calculation of the electronic structure for $BaMgAl_{10}O_{17}$ was carried out with density functional theory (DFT) and performed with the CASTEP code. The local-density approximations (LDA) based on DFT were chosen for the theoretical basis of density function. Two steps were adopted for calculating the electronic band structure of $BaMgAl_{10}O_{17}$. The first step was to optimize their crystal structure using the crystallographic data reported in Ref. [18]. The second step was to calculate its density of states for the optimized structure. For the two steps, the basic parameters were chosen as follows in setting up the CASTEP run: the kinetic energy cutoff = 450 eV, k-point spacing = 0.05 $Å^{-1}$, sets of k points = 3 × 3 × 3, SCF tolerance thresholds = 2.0×10^{-6} eV/atom, and space representation = reciprocal. The reliability of the calculation was demonstrated by the result of convergence test.

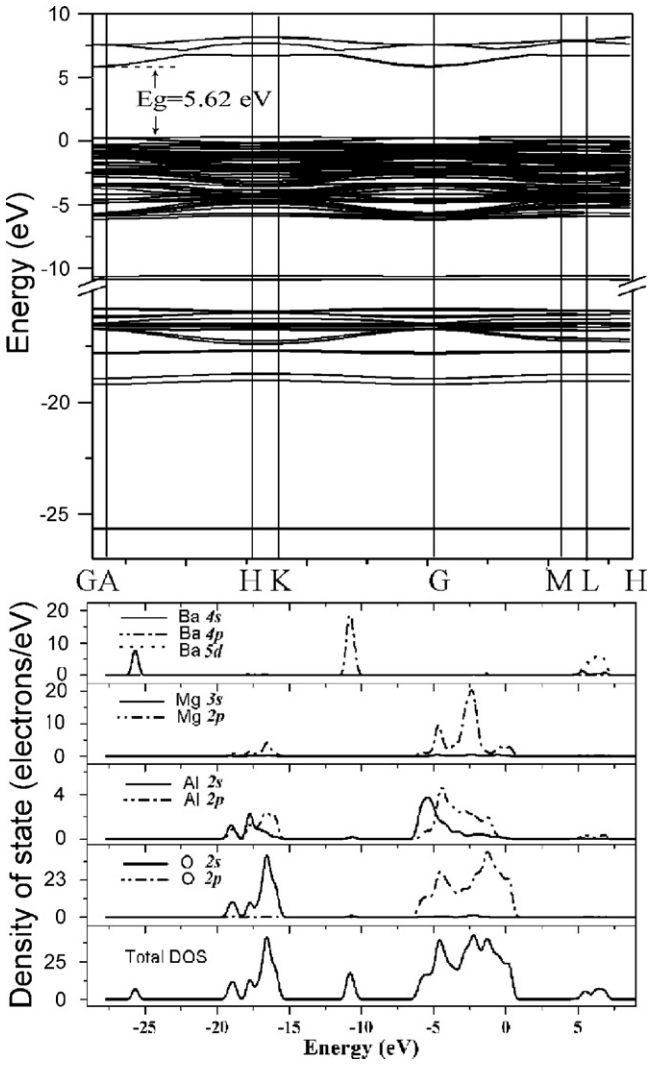

Fig. 2. Band structure and total and partial density of states of $BaMgAl_{10}O_{17}$.

3. Results and discussion

3.1. Electronic structure of $BaMgAl_{10}O_{17}$

The DFT calculation of the band structure and total and partial density of states of $BaMgAl_{10}O_{17}$ are shown in Fig. 2. The top of the valence band (VB) is at M and the bottom of the conduction band (CB) is at G, with an indirect gap of 5.62 eV. The electronic structure of the upper VB originates predominantly from O 2p and Mg 2p states, while the CB is dominantly composed of Ba 5d states. Some Al 2p and Mg 2p states sufficiently disperse within the O 2p states illuminating the covalent property of the Al–O and Mg–O bond. Only a few Al and Ba related electronic states appear in the O 2p valence band, which demonstrates ionic interaction between Al/Ba and O. On the other hand, we also calculate the band structure and total and partial density of states of $BaMgAl_{10}O_{17}$ with Si–N doping. Tough we believe N 2p would be contributed to the upper VB and make the VB is different with the un-doped one as shown in the following work, unfortunately, this work is failed due to the structure of $BaMgAl_{10}O_{17}$ is too complex even not without the Si–N doping.

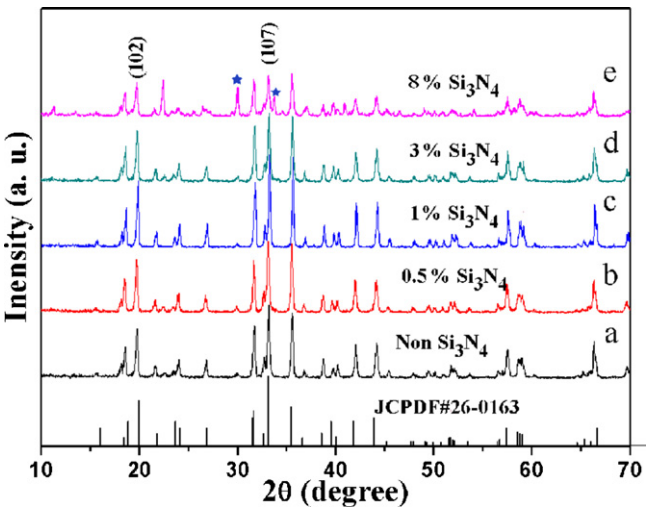

Fig. 3. XRD patterns of samples with different Si_3N_4 concentration.

3.2. X-ray diffraction analysis

The X-ray diffraction patterns of the as-prepared samples with different Si_3N_4 concentrations were depicted in Fig. 3. The XRD patterns reveal that all samples can be determined to be pure phase of BAM according to JCPDF#26-0163 shown at the bottom, except the extremely doped one (Fig. 3e, 8% Si_3N_4). The low amount of doping leads to a reduction of the unit cell parameters a and c from 5.6247 and 22.6214 Å (un-doped sample) to 5.6209 and 22.6147 Å (3% Si_3N_4), which indicates the dissolution of Si–N into the host lattice, similar to the previous results in other Al compounds [15,16]. This reduction is probably due to shorter bond lengths for tetrahedral Si–N bonds (168.5–176 pm in Si_3N_4) versus tetrahedral Al–O bonds (176.1 pm in BAM) [15]. Doping too much Si_3N_4, a few impure phases were obtained as marked in Fig. 3. A reasonable explanation is that Si_3N_4 concentrates in the surface layer of BAM due to the self-purification of BAM crystal as well as the low solution and diffusion rates of Si_3N_4 [19].

Meanwhile, the crystallite sizes of the prepared powders were calculated according to the width of (1 0 2) and (1 0 7) diffraction peak in the respective XRD patterns using the Scherrer's equation: $D = 0.941\,\lambda/\beta\cos\theta$, where D is the average grain size, λ is the X-ray wavelength (0.15405 nm), θ and β are the diffraction angle and full-width at half-maximum (FWHM) of an observed peak, respectively [20]. The results show that a monotonous increase in the crystallite sizes (4.1 μm, 5.9 μm, 6.7 μm, 7.1 μm for Fig. 3a–d, respectively) by raising the doping concentrations. It demonstrates that Si_3N_4 doping would contribute to the furtherance of the crystal growth.

3.3. SEM analysis

Fig. 3 shows the SEM images of the as-prepared samples calcined with different Si_3N_4 concentrations. The un-doped sample shows an irregularly morphology whose particle size is around 3 μm (Fig. 4a), while regular hexagonal particles and fine particle sizes (3–5 μm) are obtained by doping appropriate Si_3N_4 (Fig. 4b–c). Though their width is almost in the same range, the thickness of 1% sample (Fig. 4c) is thicker than that of the 0.5% one (Fig. 4b). For better exhibiting the morphology, one small grain is shown as inset of Fig. 4c. It has been reported that fine particles can improve aging characteristics by forming a densely packed phosphor layer and the particles of the 3–5 μm ordered showed the best luminescence

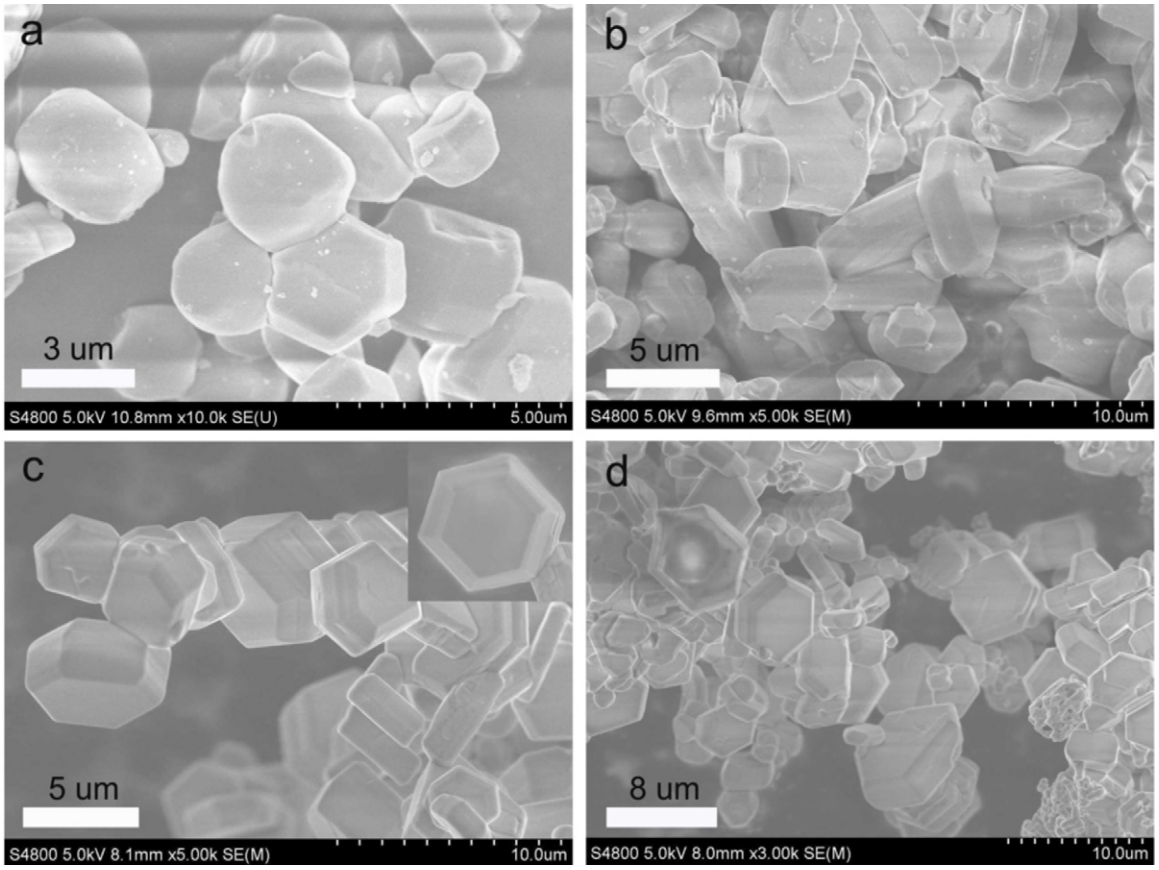

Fig. 4. SEM imagines of BAM:Eu^{2+}, Mn^{2+} phosphor with different Si_3N_4 concentration (a, non Si_3N_4; b, 0.5% Si_3N_4; c, 1% Si_3N_4; d, 8% Si_3N_4).

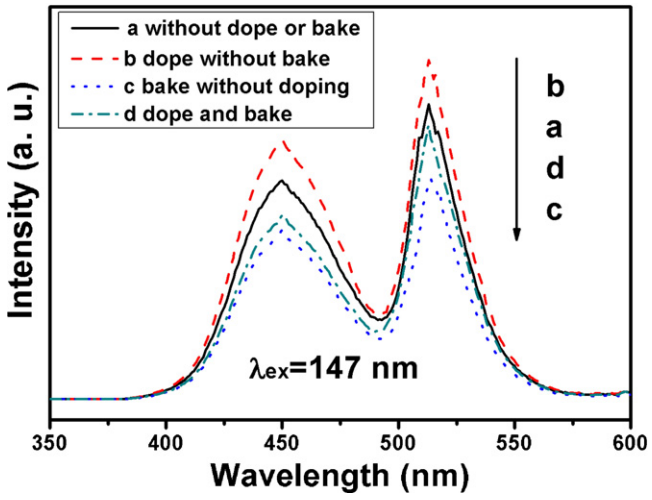

Fig. 5. Emission spectra of BAM:0.1Eu^{2+}, 0.12Mn^{2+} with and without Si_3N_4 doping before and after bake.

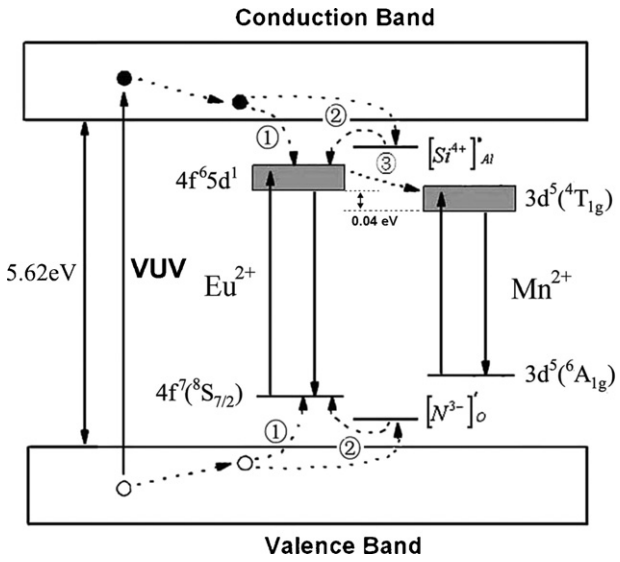

Fig. 6. Energy levels of the BAM:Eu^{2+}, Mn^{2+} with Si_3N_4 doping.

characteristics [21]. There would be a potential application of our observed result. When the concentration increases to 8%, the particles show agglomerate and irregularly. It is obviously illustrated that a suitable amount of Si_3N_4 doping would accelerate the crystal growth and achieves fine particle morphology.

3.4. Photoluminescence properties

In order to study the sensitizing of BAM:Eu^{2+}, Mn^{2+} by Si_3N_4 doping, the emission spectra of Si–N-doped and undoped sample before and after annealing process are shown in Fig. 5. As can be seen clearly the emission spectra of BAM:0.1Eu^{2+}, 0.05Mn^{2+} with and without 1% Si_3N_4 concentrations were measured as Fig. 5a and b shown. The result shows that the emission intensity is enhanced by Si_3N_4 doping. It clearly illustrates that Eu^{2+} emission peaked at 450 nm increases 17.3% while the Mn^{2+} emission peaked at 515 nm increases 14.4% with 1% Si_3N_4 doping. The enhancement of Eu^{2+} emission would illustrate in the later pages. However, as is well known, Si–N tetrahedron would substitute some Mn^{2+} sites owing to Mn^{2+} occupies Mg^{2+} which locates in Al(Mg)O_4 tetrahedron. This would result in a decreasing of the photoluminescence of Mn^{2+} emission, which deviates the observed result. It implies that there should be a secondary effect associated with Mn^{2+} emission. For a better understanding of this phenomenon, a energy level of Si_3N_4 doping BAM:Eu, Mn was list as Fig. 6 shows. As mentioned, tetrahedral Al–O would be replaced by Si–N tetrahedron, and the substitution would occur as below:

$$Al^{3+} + Si^{4+} \rightarrow [Si^{4+}]^{\bullet}_{Al} \quad (1)$$

$$O^{2-} + N^{3-} \rightarrow [N^{3-}]'_{O} \quad (2)$$

As shown in Fig. 6, the energy levels of $[Si^{4+}]^{\bullet}_{Al}$ close to the conduction band of the host, and the holes are captured from the conduction band. The energy level of $[N^{3-}]'_{O}$ is close to the valence band, and the electrons are captured from the valence band. As a result, $[N^{3-}]'_{O}$ would act as a donor of electrons, while $[Si^{4+}]^{\bullet}_{Al}$ become acceptors of the electrons. Consequently, under the combined action of $[Si^{4+}]^{\bullet}_{Al}$ and $[N^{3-}]'_{O}$, the electrical neutrality of the compounds would be maintained, and the holes in the valence band and the electrons in the conduction band increase similar to Zhang's work [22]. The possibility for the excited state of Eu^{2+} and Mn^{2+} to capture electrons and the ground state to capture the holes would be higher (as process (1) in Fig. 6) than the un-doped sample (as process (3) in Fig. 6), so that the luminescent intensity increases. When too large of Si–N ions doped into phosphor, the defects will associate. As a result, the luminescent intensity decreases again (as Fig. 5 shows). However, what interested us is the energy transfer between Eu^{2+} and Mn^{2+}. In our hypothesis, Si–N tetrahedron would substitute some Mn^{2+} site owing to Mn^{2+} ions were occupied Mg^{2+} ions which located in Al(Mg)O_4 tetrahedron. This would result a photoluminescence decrease in Mn^{2+} emission (peak at 515 nm). However, the intensity of Mn^{2+} emission (peak at 515 nm) increases 14.4% while Eu^{2+} emission (peak at 450 nm) enhanced 18.3%. It means that the energy transfer from Eu^{2+} to Mn^{2+} would become more efficiently as process (3) in Fig. 6. Then, this phenomenon could be explained by this hypothesis. In additionally, it obvious that the Si–N doped sample exhibits a better thermal stability when samples suffer a heat treatment in air for 1 h as Fig. 5c and d shown. The stronger emission intensity of Si–N doped sample suffered a heat treatment may be attributed to following reasons: first, the substitution of Si–N tetrahedron for tetrahedral Al–O would result in smaller crystal lattices which would restrict the movement of activators. Secondly, lower electro negativity of nitrogen ions can effectively avoid the divalent Eu oxidized to trivalent Eu [15,23]. Thirdly, the smaller lattice would impact the energy transfer efficient between Mn^{2+} and Eu^{2+} [24].

3.5. Decay curves analysis

To better understand the effect of Si–N doping on the energy transfer from Eu^{2+} to Mn^{2+}, the decay curves were measured which presented in Fig. 7 to calculate energy transfer efficiency ($\eta\tau$) from Eu^{2+} to Mn^{2+} by:

$$\eta\tau = 1 - \frac{\tau_S}{\tau_{S0}} \quad (3)$$

where τ_{S0} is the decay time of Eu^{2+} of the phosphor in the absence of Mn^{2+}, and τ_S is the decay time of Eu^{2+} in the presence of Mn^{2+}. It clearly shows that with the doping concentration increasing, a slightly shorter decay time τ_S can be achieved. It could be contributed that doping with Si–N would result the lattice smaller, and impacted the energy transfer efficient between Mn^{2+} and Eu^{2+} [24]. As a result, the $\eta\tau$ increased from 0.55 to 0.69 (in the inset of Fig. 7) which demonstrated the energy transfer from Eu^{2+} to Mn^{2+} indubitably enhanced.

Because the energy transfer from Eu^{2+} to Mn^{2+} is consider as a dipole-quadruple mechanism, the critical distance R_c for the energy

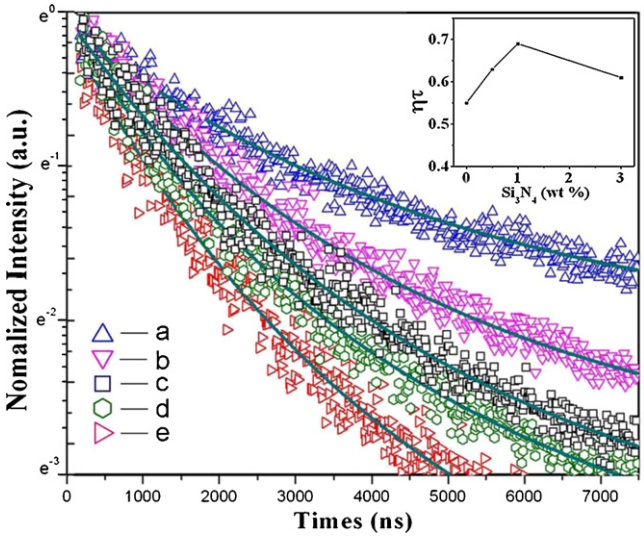

Fig. 7. Decay curves of samples with different Si_3N_4 concentration (a, BAM:0.1Eu^{2+}, without Si_3N_4 doping; b, BAM:0.1Eu^{2+}, 0.12Mn^{2+}, without Si_3N_4 doping; c, BAM:0.1Eu^{2+}, 0.12Mn^{2+}, 3% Si_3N_4; d, BAM:0.1Eu^{2+}, 0.12Mn^{2+}, 0.5% Si_3N_4; e, BAM:0.1Eu^{2+}, 0.12Mn^{2+}, 1% Si_3N_4). Inset: the energy transfer efficiency $\eta\tau$ dependence on Si_3N_4 concentration.

transfer from Mn^{2+} was calculated by [25]:

$$R_c^8 = 0.63 \times 10^{28} \times \frac{f_q \lambda_S^2 Q_A}{f_d E_S^4} \int F_S(E) F_A(E) dE \quad (4)$$

where $Q_A = 4.8 \times 10^{-16} f_d$ is the absorption cross section of Mn^{2+}, $f_d = 10^{-7}$ and $f_q = 10^{-10}$ are the oscillator strengths of the dipole and quadruple electrical absorption transitions for Mn^{2+}; $\lambda_S = 4500$ Å and $E_S = 2.8$ eV are the emission wavelength and emission energy of Eu^{2+}, respectively, and $\int F_S(E)F_A(E)dE$ expresses the spectral overlap between the normalized shapes of Eu^{2+} emission $F_S(E)$ and Mn^{2+} excitation $F_A(E)$, and it is estimated at about 1.82 eV^{-1}. Therefore, the *RC* for energy transfer Eu → Mn in BAM:Eu^{2+}, Mn^{2+} was reckoned to be 9.7 Å, which is slightly smaller than Ke's work (10.9 Å) [26]. It also demonstrates that a more efficient energy transfer from Eu^{2+} to Mn^{2+} can be obtained by suitable Si–N doping.

4. Conclusions

Si–N doped BAM:Eu^{2+}, Mn^{2+} phosphors were synthesized by a conventional solid-state reaction, and its photoluminescence properties were studied. The calculated results which obtained by using the density functional theory shows $BaMgAl_{10}O_{17}$ possesses an indirect optical band gap about 5.62 eV. The upper VB and the lower CB are decided by O/Mg 2p and Si 2p states, respectively. Suitable Si–N doping could result in a regular morphology and size. In addition, Si–N doping leading to an increase in luminance intensity and thermal stability, which could be attributed to the lower electro negativity of nitrogen and a newly formed defect energy level. Due to the smaller lattice with Si–N doping, the energy transfer from Eu^{2+} to Mn^{2+} also becomes more effectively. These are expected to be potentially applicable to industrial production of the phosphor in plasma display panels.

Acknowledgement

This work was supported by the National Science Foundation for Distinguished Young Scholars (No. 50925206), the National Natural Science Foundation of China (No. 10874061) and the Research Fund for the Doctoral Program of Higher Education (No. 200807300010).

References

[1] S. Oshio, T. Matsuoka, S. Tanaka, H. Kobayashi, J. Electrochem. Soc. 145 (1998) 3898–3902.
[2] S. Ekambaram, K.C. Patil, J. Alloys Compd. 248 (1997) 7–12.
[3] P. Zhu, W. Di, Q. Zhu, B. Chen, H. Zhu, H. Zhao, Y. Yang, X. Wang, J. Alloys Compd. 454 (2008) 245–249.
[4] Z. Zhang, Y. Wang, X. Li, J. Alloys Compd. 478 (2009) 801–804.
[5] Z. Wang, Y. Wang, Y. Lia, B. Liu, J. Alloys Compd. 506 (2011) 343–346.
[6] B. Howe, A.L. Diaz, J. Lumin. 109 (2004) 51–59.
[7] K.S. Sohn, S.S. Kim, H.D. Park, Appl. Phys. Lett. 81 (2002) 1759–1761.
[8] H. Yamada, W.S. Shi, C.N. Xu, J. Electrochem. Soc. 151 (2004) 349–351.
[9] T.H. Kwon, M.S. Kang, J.P. Kim, G.J. Kim, J. Soc. Inf. Disp. 10 (2002) 241–245.
[10] B. Dawson, M. Ferguson, G. Marking, A.L. Diaz, Chem. Mater. 16 (2004) 5311–5317.
[11] B. Liu, Y. Wang, F. Zhang, Y. Wen, Q. Dong, Z Wang, Opt. Lett. 35 (2010) 3072–3074.
[12] K.H. Lee, J.H. Crawford Jr., Appl. Phys. Lett. 33 (1978) 273–275.
[13] R. Ramírez, M. Tardío, R. Gonzàlez, J.E. Muñoz Santiuste, J. Appl. Phys. 101 (2007) 123520–123521.
[14] K.C. Mishra, K.H. Johnson, P.C. Schmidit, J. Electrochem. Soc. 153 (2006) 202–208.
[15] Y. Wang, X. Xu, L. Yin, L. Hao, J. Am. Ceram. Soc. 93 (2010) 1534–1536.
[16] A.A. Setlur, W.J. Heward, M.E. Hannah, U. Happek, Chem. Mater. 20 (2008) 6277–6283.
[17] T. Justel, H. Lade, W. Mayr, A. Meijerink, D. U Wiechert, J. Lumin. 101 (2003) 195–210.
[18] Z.D. Sharp, R.M. Hazen, L.W. Finger, Am. Mineral. 72 (1987) 748–755.
[19] J.S. Kim, P.E. Jeon, Y.H. Park, J.C. Choi, H.L. Park, G.C. Kim, T.W Kim, Appl. Phys. Lett. 85 (2004) 3696–3698.
[20] T. Kojima, in: S. Shionoya, W.M. Yen (Eds.), Phosphor Handbook, CRC, Boca Raton, 1999.
[21] F. Bondioli, A.B. Corradi, T. Manfredini, Chem. Mater. 12 (2000) 324–330.
[22] J. Zhang, Z. Zhang, Z. Tang, Y. Tao, X. Long, Chem. Mater. 14 (2002) 3005–3008.
[23] X. Xu, T. Nishimura, Q. Huang, R.J. Xie, N. Hirosaki, H. Tanaka, J. Am. Ceram. Soc. 90 (2007) 4047–4049.
[24] J. Zhou, Y. Wan, B. Liu, Y Lu, J. Alloys Compd. 484 (2009) 439–443.
[25] W.J. Yang, L. Luo, T.-M. Chen, N.S Wang, Chem. Mater. 17 (2005) 3883–3888.
[26] W. Ke, C. Lin, R. Liu, M Kuo, J. Electrochem. Soc. 157 (2010) 1307–1309.